Cell

EXTENDED EXPERIMENTAL PROCEDURES

Plasmids and Constructs Used

All constructs for mammalian expression were cloned into the pHR lentiviral backbone (kindly provided by John R. James). Phy-mCherry-CAAX was cloned from a retroviral construct used previously (Toettcher et al., 2011a). pHR YFP-PIF-SOScat was constructed by PCR amplification of YFP-PIF from a previously used retroviral vector (Toettcher et al., 2011a) and human SOS2 (kindly provided by Wilson Wong) using the In-Fusion enzyme cocktail (Clontech) to insert both into the pHR backbone. pHR TagBFP-Erk2 was constructed by PCR amplification of Erk2 from a GFP-Erk2 plasmid (kindly provided by H. Steven Wiley) and TagBFP (kindly provided by Ron Vale). pHR TagBFP-PIF-SOScat was constructed by PCR amplification of TagBFP and insertion into pHR YFP-PIF-SOScat cut with BamHI (kindly provided by Wilson Wong) using the In-Fusion enzyme cocktail (Clontech) to insert both into the pHR backbone.

Lentivirus was produced by cotransfecting the pHR plasmids and vectors encoding packaging proteins (pMD2.G and p8.91) using the Fugene 6 HD transfection reagent in HEK293 cells plated in 6-well plates at ~70% confluency. Viral supernatants were collected 2 days after transfection and 0.45 μm filtered. Supernatant was used for transduction immediately, stored at 4 degrees for up to 2 weeks, or kept at −80 degrees for long-term storage.

Retroviral and Lentiviral Transduction

NIH 3T3 cells (ATCC) were cultured in 10% fetal bovine serum (UCSF Cell Culture Facility) in DMEM (Invitrogen) supplemented with penicillin, streptomycin and glutamine at 37°C with 5% CO2 in a humidified incubator. For viral transduction, NIH 3T3 cells were plated in 6-well dishes to achieve ~20% confluency at the time of infection. For lentiviral transduction, 10–100 μl of each virus' supernatant was added directly to cells. Viral media was replaced with normal growth media 24 hr post infection. Cells were sorted for coexpression of each fluorescent construct by fluorescence-activated cell sorting on a FacsAria2 (Beckton-Dickinson), and a bulk-sorted population consisting of fluorescence positive cells was used for each experiment.

Preparing Cells for Imaging

For imaging and immunofluorescence experiments, 8-well chambered glass slides (Nunc; Lab-Tek) were coated for 1 hr with 100 μl of 0.08 mg/ml fibronectin (which we prepared from whole porcine blood), then washed with PBS. 40,000 cells were plated on each dish in normal growth media and allowed to adhere for at least 30 min. For experiments requiring cell starvation, cells were starved overnight in DMEM supplemented with glutamine, penicillin, streptomycin, and 20 mM HEPES buffer. For light stimulation experiments, cells were incubated for 30 min with 4 μM phycocyanobilin (PCB, extracted from Spirulina [Toettcher et al., 2011b]; 4 mM stock was prediluted into conditioned media and added to dishes in the dark).

Microscopy

All images for light recruitment experiments were taken on a microscope with a custom built environmental chamber with temperature and CO2 control (In Vivo Scientific) on a Nikon Eclipse Ti inverted microscope equipped with a Yokogawa CSU-X1 spinning disk confocal, a 40× PlanApo TIRF 1.49 NA objective, and an electron microscopy charge-coupled device (EM-CCD) camera (Andor). 405 nm, 488 nm, and 561 nm laser wavelengths (LMM5, Spectral Applied Research) were used for excitation.

To expose cells to variable 650 and 750 nm light intensities for optogenetic control, we used a 650 nm LED (Lightspeed Technologies) placed in the epifluorescence illumination port and a 750 nm long-pass glass filter (FSQ-RG9, Newport) placed in the bright-field light path. To implement software-based voltage control of light intensity, we connected the 650 nm LED to the analog outputs of a DT9812 board (Data Translation) and controlled its voltages over time using custom MATLAB code (Toettcher et al., 2011a), while simultaneously leaving the diascopic shutter open to globally illuminate the sample with 750 nm light.

Image Processing

To analyze live-cell time-lapse movies of nuclear Erk and membrane SOScat, we measured the mean nuclear BFP-Erk and cytoplasmic PIF-YFP-SOScat intensity manually in single cells at each time point using ImageJ. The background intensity of a non-cell region was subtracted from these trajectories. Each trajectory was then processed using the data processing pipeline described in Figure S2D.

We found that for control cells (ones not undergoing light-based activity changes), two factors lead to background changes in measured fluorescence over time: (1) photobleaching, which leads to an exponential decay in fluorescence intensity while images are being acquired, and (2) cells movement and shape changes occurring over many hours of stimulation that can change the baseline fluorescence intensity in the cytoplasm and to a lesser extent the nucleus, whose shape is more constant over time (raw trajectories in Figures S2E and S3A). To correct for these background effects, we subtracted a 75 min moving average from each trajectory (long enough to average over multiple recruitment/derecruitment cycles for the dose response and frequency-response experiments) (Figures S2F and S3B). This correction leads to a signal with zero mean whose variations represent time dependent changes in Erk nuclear recruitment or SOScat cytoplasmic depletion. To correct for the fact that photobleaching still leads to an exponential time decay in the envelope of this variation, we multiply by a correction term which is the inverse of the bleaching-induced exponential decay.

Using these corrected images, we measured the observed decrease in cytoplasmic SOScat and inverted this signal to calculate the increase in SOScat at the membrane (Figures S2G and S3C). Although we are ultimately most interested in the amount of SOScat that is recruited to the membrane upon light stimulation, we focused on measuring changes in cytoplasmic SOScat because of technical constraints, discussed below. We also have shown in control experiments discussed below that SOScat cytoplasmic depletion accurately represents the inverse of SOScat membrane recruitment. Although techniques do exist to directly measure SOScat membrane recruitment (e.g., TIRF microscopy, which provides direct measurement of the membrane fluorescence above the coverslip), we were technically unable to use these approaches in conjunction with acquiring confocal timelapse images of Erk nuclear translocation (our signaling reporter in live-cell experiments). Confocal imaging can be used, however, to rapidly and accurately measure both the change in cytoplasmic SOScat and the change in nuclear Erk, the two measurements that we have used in our analysis. Confocal microscopy can in principle be used to measure either light-induced *increase* in membrane fluorescence and *decrease* in cytoplasmic fluorescence in optogeneticaly stimulated cells (Figure S2A). A confocal line scan though an individual cell (Figure S2A; gold line) shows an increase in membrane fluorescence that is related to the intensity of red light applied (Figure S2B). We can use these direct line scan measurements to show that there is a good empirical correlation between measuring cytoplasmic depletion and membrane recruitment. Direct measurements of membrane recruitment showed a quantitative increase that was closely related to the level of cytoplasmic depletion, with both techniques showing a similar $K_{1/2}$ of about 0.2 V 650 nm light (Figure S2C). Technically we choose to measure cytoplasmic depletion of SOScat because it proved to be less noisy than quantifying the membrane increase from line scans (the cytoplasmic measurement uses more pixels). Thus cytoplasmic depletion was measured throughout this work.

Finally, for single-cell dose-response curves, each cell's trajectory is then offset from the zero-mean value by noting that inactivating light drives a membrane recruitment value of 0 (we do not observe PIF recruitment in the absence of light) and that the nuclear Erk fold-change of unstimulated cells is defined to be 1 (Figure S2H). Frequency-response trajectories are left as zero-mean signals for Fourier analysis. All data analysis was performed in MATLAB using custom scripts implementing built-in functions (e.g., Fourier analysis was performed using: fft()).

Cell Lysate Preparation for Western Blots and RPPA Analysis

For all western blots and RPPA experiments, 5×10^6 cells were plated in wells of a 6-well plate (or standalone 3 cm dishes if individual light stimuli were required), and serum starved overnight in DMEM + penicillin, streptomycin, glutamine, and 20 mM HEPES. At appropriate time points after stimulation, wells were washed once with ice-cold PBS and lysed in 150 μl ice-cold lysis buffer (1% Triton X-100, 50 mM HEPES, pH 7.4, 150 mM NaCl, 1.5 mM $MgCl_2$, 1 mM EGTA, 100 mM NaF, 10 mM Na pyrophosphate, 1 mM Na3VO4, 10% glycerol, and freshly added protease and phosphatase inhibitors from Roche Applied Science Cat. # 05056489001 and 04906837001, respectively) and incubated on ice with occasional shaking for 20 min. Cells and lysis buffer were scraped off each well, collected in 1.5 ml Eppendorf tubes and centrifuged at 13,000 g at 4°C for 10 min. After protein quantification by BCA assay, 50 μl of SDS sample buffer (40% glycerol, 8% SDS, 0.25M Tris-HCL, pH 6.8, 10% 2-mercaptoethanol) was added and samples were boiled for 5 min. Samples were then frozen at −80°C or loaded immediately onto gels for western blot processing.

Western Blots

For western blots, lysates were loaded into 17-well precast 4%–12% Bis-Tris gels (Invitrogen) and run at 140 V for 1 hr. Gels were transferred for 1 hr onto nitrocellulose membranes using a Trans-Blot semi-dry transfer apparatus (Bio-Rad). Membranes were blocked in Odyssey blocking buffer (Li-Cor) for > 1 hr, exposed to primary antibodies diluted 1:1,000 in Odyssey buffer for 2 hr at room temperature or overnight at 4°C, washed in TBST, and exposed to IRDye (Li-Cor) fluorescent anti-rabbit and anti-mouse secondary antibodies at 1:10,000 dilution in Odyssey buffer for 1 hr. Membranes were then imaged on a Li-Cor imaging station and band intensities quantified in ImageJ. Primary antibodies used were rabbit anti-phospho-Erk1/2 (Cell Signaling Ab #4370), rabbit anti phospho-STAT3 (Cell Signaling Ab #9145), rabbit anti-phospho Akt (Cell Signaling Ab #9271), rabbit anti-phospho c-Fos (Cell Signaling Ab #5348), rabbit anti-c-Fos (Cell Signaling Ab #2250), mouse anti-Erk2 (Santa Cruz Ab #1647), and mouse anti-α-tubulin (Sigma Aldrich, clone B-5-1-2).

RPPA Analysis

Cell lysates were sent to the MD Anderson Cancer Center's facility for RPPA analysis, where they were denatured by 1% SDS (with beta-mercaptoethanol) and diluted in five 2-fold serial dilutions in dilution buffer (lysis buffer containing 1% SDS). Serial diluted lysates were arrayed on nitrocellulose-coated slides (Grace Biolab) by Aushon 2470 Arrayer (Aushon BioSystems). Total 5,808 array spots were arranged on each slide including the spots corresponding to positive and negative controls prepared from mixed cell lysates or dilution buffer, respectively.

Each slide was probed with a validated primary antibody plus a biotin-conjugated secondary antibody. Only antibodies with a Pearson correlation coefficient between RPPA and western blotting of greater than 0.7 were used in the reverse phase protein array study. Antibodies with a single or dominant band on western blotting were further assessed by direct comparison to RPPA using cell lines with differential protein expression or modulated with ligands/inhibitors or siRNA for phospho- or structural proteins, respectively. The signal obtained was amplified using a Dako Cytomation–catalyzed system (Dako) and visualized by DAB colorimetric reaction. The slides were scanned, analyzed, and quantified using a customerized-software Microvigene (VigeneTech Inc.) to generate spot intensity.

Each dilution curve was fitted with a logistic model (“Supercurve Fitting” developed by the Department of Bioinformatics and Computational Biology in MD Anderson Cancer Center, “http://bioinformatics.mdanderson.org/OOMPA”). This fits a single curve using all the samples (i.e., dilution series) on a slide with the signal intensity as the response variable and the dilution steps are independent variable. The fitted curve is plotted with the signal intensities—both observed and fitted—on the y axis and the $\log_2$-concentration of proteins on the x axis for diagnostic purposes. The protein concentrations of each set of slides were then normalized by median polish, which was corrected across samples by the linear expression values using the median expression levels of all antibody experiments to calculate a loading correction factor for each sample.

Finally, to account for noise between biological replicates for each protein in the RPPA array, linear expression levels were normalized to the standard deviation across all biological replicates of the untreated condition.

Immunofluorescence Assays

For immunofluorescence assays, cells were plated on fibronectin-coated 8-well chambered coverslips (Nunc; Lab-Tek) and starved overnight, as described for imaging above. Cells were stimulated with PCB + light or ligand. At the appropriate time, serum was removed and cells were fixed with 4% paraformaldehyde (CytoFix, BD) at 4°C for 15 min. After 1 wash with PBS, cells were permeabilized in ice-cold 90% methanol at −20°C for 10 min. Cells were then washed once in PBS, blocked in IF buffer (PBS + 10% fetal bovine serum + 2 mM EDTA) for 1 hr, and incubated overnight in primary antibody diluted 1:100 into IF-T buffer (IF buffer + 0.3% v/v Triton-X) at 4°C. The next day, wells were washed 3 × 5 min in IF-T buffer, incubated for 1 hr in Alexa 488-conjugated goat anti-rabbit secondary antibody diluted 1:100 in IF-T buffer (Invitrogen catalog #A11008), and washed 3 × 5 min in IF-T buffer before being resuspended in IF buffer for immediate imaging by confocal microscopy.

SUPPLEMENTAL REFERENCES

Levskaya, A., Weiner, O.D., Lim, W.A., and Voigt, C.A. (2009). Spatiotemporal control of cell signalling using a light-switchable protein interaction. Nature *461*, 997–1001.

Toettcher, J.E., Gong, D., Lim, W.A., and Weiner, O.D. (2011a). Light-based feedback for controlling intracellular signaling dynamics. Nat. Methods *8*, 837–839.

Toettcher, J.E., Gong, D., Lim, W.A., and Weiner, O.D. (2011b). Light control of plasma membrane recruitment using the Phy-PIF system. Methods Enzymol. *497*, 409–423.

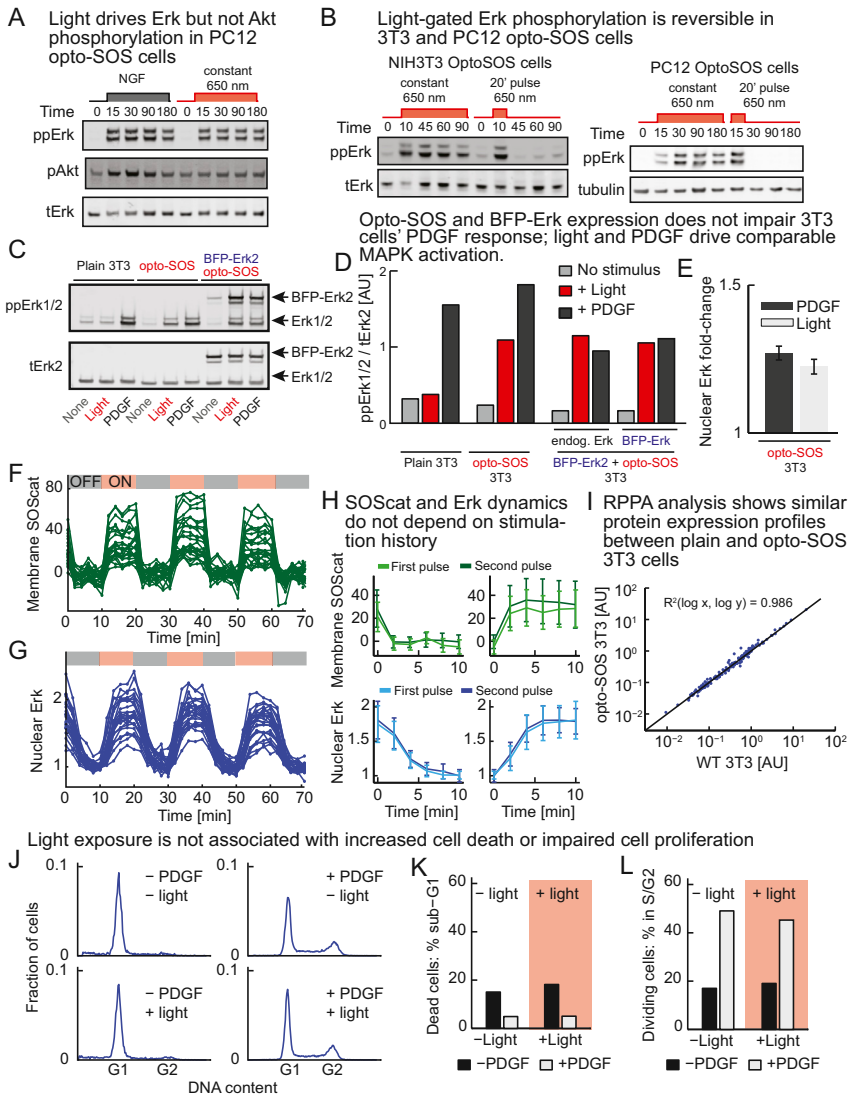

Figure S1. Optogenetic Activation of Ras/Erk Signaling Is Fast and Reversible in Cells, Related to Figure 2

(A) PC12 opto-SOS cells were stimulated with a saturating 100 ng/ml NGF dose or constant 650 nm light and were blotted for phospho-Akt (pAkt) and doubly phosphorylated Erk (ppErk). NGF activates both Erk and Akt, while light is specific for Erk. NGF and light both drive similar levels of Erk activation.

(B) Light-dependent Erk phosphorylation is quickly reversible in both NIH 3T3 and PC12 opto-SOS cells. Lysates were collected from cells stimulated by sustained or transient activating light pulses, and blotted for ppErk. In both lines, Erk phosphorylation is reversible after the light pulse.

(C and D) Expression of opto-SOS and TagBFP-Erk do not significantly alter the cell's response to growth factor. Plain 3T3s, opto-SOS 3T3s, and opto-SOS/reporter 3T3s were left untreated or stimulated with light or growth factor, and blotted for ppErk (C). Ratio of phospho to total Erk was quantified in each case, and a similar ratio of ppErk/total Erk is induced by PDGF in each line (D). Light activates opto-SOS lines similarly, whereas plain 3T3s are not stimulated by light (D).

(E) Light and PDGF drive similar levels of Erk nuclear translocation in opto-SOS cells. Quantification is shown of the peak BFP-Erk nuclear translocation observed in opto-SOS cells stimulated by light or PDGF (mean + SEM).

(F–H) The kinetics and levels of light-stimulated membrane SOScat and nuclear Erk do not depend on prior stimuli. Membrane SOScat recruitment (F) and nuclear localization of fluorescent Erk (G; TagBFP-Erk) are quickly reversible after activating or inactivating light treatment. Single-cell trajectories of membrane SOScat and nuclear Erk were measured from 25 individual cells during 10 min pulses of 650 nm and 750 nm light. The mean + SD of the trajectories in (F) and (G) were quantified in response to the first two activating and inactivating light pulses (H).

(I) Expression of the opto-SOS system does not induce major changes to overall cell behavior. Reverse phase protein array analysis (see Figure 5; Figure S4) shows highly correlated levels (R2 = 0.986) of a panel of 180 total and phospho-proteins from lysates collected from unstimulated plain 3T3 cells and opto-SOS 3T3 cells.

(J–L) The red/infrared light applied to drive optogenetic activation neither inhibits cell division nor induces cell death. (J) Flow cytometry histograms of cells fixed and PI stained for DNA content show G1 arrest and S-G2 progression in response to PDGF. (K) Events with less than G1 DNA content is indicative of cell death: this sub-G1 cell population is not increased by light exposure in either serum-starved or PDGF-stimulated cells. (L) Cell-cycle progression was ascertained by measuring the fraction of cells in S and G2 cell cycle states 16 after PDGF-induced cell-cycle reentry: again, light did not change the fraction of cells progressing through S and G2 after PDGF stimulation.

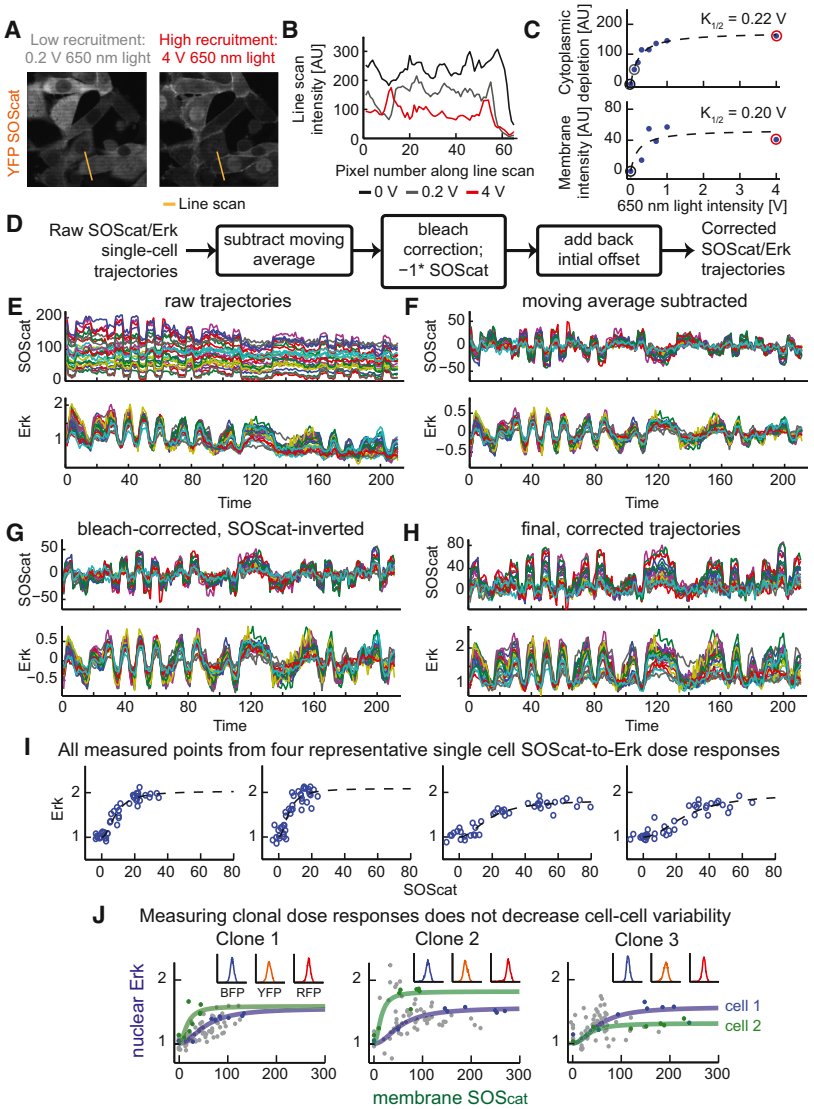

Figure S2. Extracting Single-Cell Dose Information from Live-Cell Trajectories, Related to Figure 3

(A–C) Measuring SOScat cytoplasmic depletion after light stimulation provides quantitative information about membrane accumulation. (A) YFP-PIF-SOScat was measured by confocal fluorescent microscopy in 3T3 opto-SOS cells after 1 min of 650 nm light exposure. Both depletion of fluorescent SOScat from the cytoplasm and an increase on the membrane (seen on the border of each cell) can be observed by eye (A) and quantified along a line scan through an individual cell (B). (C) Plotting the membrane accumulation along the line scan (intensity peaks on each side in B) or its cytoplasmic depletion (the mean intracellular intensity in B) show highly correlated dependencies on light intensity, with measured K1/2 values with less than 10% difference. We choose to measure cytoplasmic depletion because (1) it is calculated from a large number of pixels and is therefore less noisy (compare upper and lower panels of C), and (2) does not require identification of a small number of border pixels representing the cell membrane.

(D) Schematic of the data-processing pipeline for single-cell membrane SOScat and nuclear Erk trajectories.

(E–H) All cell trajectories are shown as raw data, and after each data processing step. Raw cytoplasmic YFP-PIF-SOScat and nuclear TagBFP-Erk intensities are measured from confocal images each minute for ~4 hr (shown in E). To account for changes in cell size and morphology over time, the mean intensity of a 50 min sliding window is subtracted from each trajectory (shown in F). Photobleaching is corrected by multiplying each subtracted trajectory by an exponential, and membrane accumulation of SOScat is measured by inverting cytoplasmic depletion (shown in G). Finally, the offset for each trajectory is added back, so zero light input corresponds to no membrane SOScat of 0 and a fold-change nuclear Erk of 1 (shown in H).

(I) Dose-response data measured from each cell are highly quantitative and reproducible. All data points measured from four representative single cells are shown, as processed in (E)–(H) and analyzed in Figure 3. The membrane SOScat and nuclear Erk intensity for each light dose is shown. Black dotted lines are best-fit Hill curves with a Hill coefficient = 2 and where the K1/2 and amplitude are allowed to vary for each cell.

(J) Cell-cell variability does not arise through optogenetic component genomic integration site or expression level. Dose response curves were measured from each of three clonally derived opto-SOS 3T3 cell lines. In each case, data from 10 cells are shown (gray points) and two representative cells are highlighted (blue and green points; best-fit lines were computed as in I). Inset figures show flow cytometry histograms of BFP-Erk, YFP-PIF-SOScat and Phy-mCherry-CAAX expression in each clonal cell line—expression is tightly controlled within each clone.

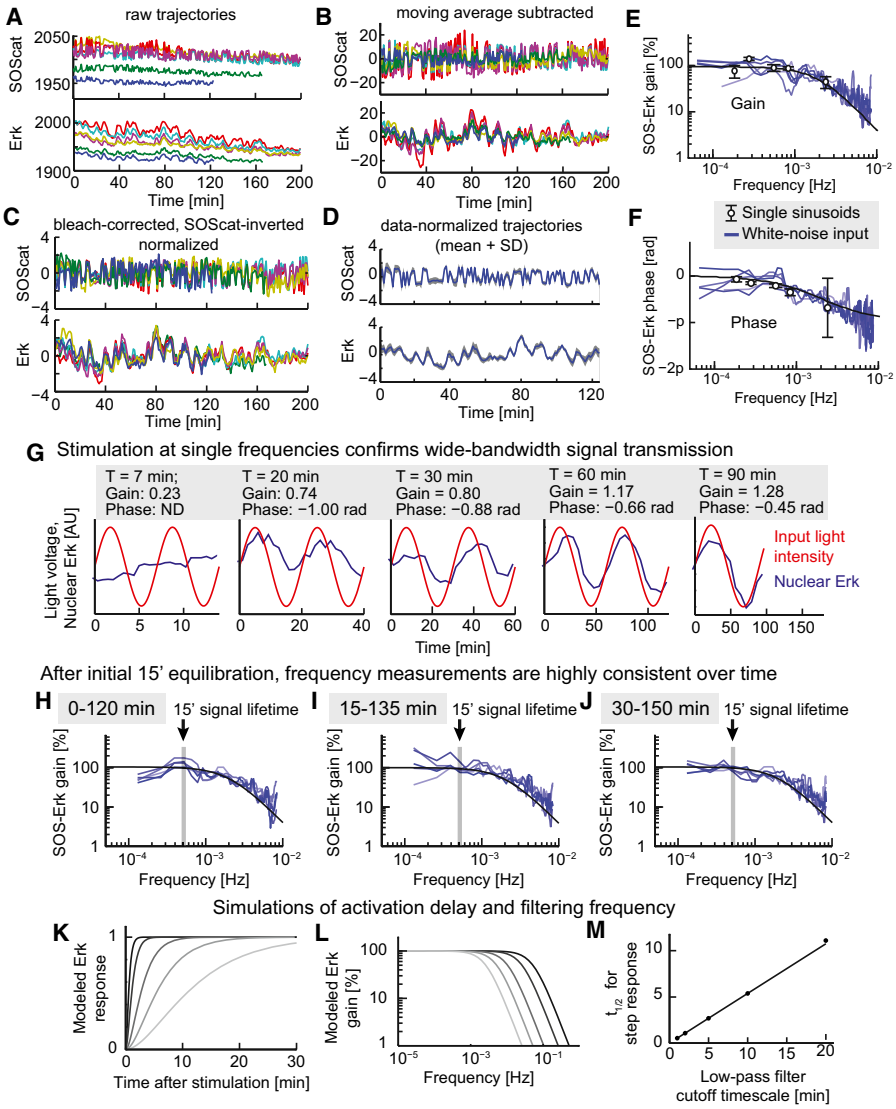

Figure S3. Extracting Single-Cell Frequency-Response Information from Live-Cell Trajectories, Related to Figure 4

(A–D) Data processing, as described in Figures S2E–S2H, applied to the single-cell frequency-response measurements described in Figure 4. (A) Raw cytoplasmic YFP-PIF-SOScat and nuclear TagBFP-Erk intensities are measured from confocal images in five cells once per minute for over 3 hr. (B) To account for changes in cell size and morphology over time, the mean intensity of a 1 hr sliding window is subtracted from each trajectory. (C) Photobleaching is corrected by multiplying each subtracted trajectory by an exponential, and membrane accumulation of SOScat is measured by inverting cytoplasmic depletion. (D) Each cell responds with highly similar kinetics and levels. The mean + SD across all six cells is shown at each time point during the first 2 hr.

(E and F) The full gain and phase frequency-response curves for each cell (reflected in the gain-only frequency response shown in Figure 4). The frequency-response gain and phase found by computing the Fourier transform of the signals in (C). Solid black lines show the relationship predicted by a single-parameter 2nd order linear model (see Extended Experimental Procedures). Solid white circles and error bars (mean + SD) show gains and phases measured using sinusoidal inputs at specific frequencies delivered to each cell, discussed further in (G).

(G) Driving cells with sinusoidal inputs at specific frequencies provides an alternate approach for measuring the frequency response. Results are shown from one representative cell, comparing the light input delivered (red line) and nuclear Erk response (blue line). For each frequency, the measured gain and phase are also indicated (text over gray background).

(H–K) Frequency analysis performed on different time-windows of the total noisy trajectories shown in (C) suggests subtle changes in the frequency response after initial time points. In each plot, the SOScat-to-Erk gain is computed as in (E) and Figure 4, but only from subsets of the total timecourse in (C). Solid black lines show the same linear filter model in (E) and Figure 4. Some amplification of frequency signals in the 15 min range is observed in the 0–120 min frequency response (H), but the frequency response at later times is flat across this frequency range (I–K). These differences may reflect initial transient behavior from the pathway as it approaches the steady state driven by the time-varying input.

(K–M) Model predictions of the relationship between the mean delay time through a simple linear low-pass filter, and its cutoff frequency. (K) Simulations showing the predicted kinetics of Erk activation in response to a constant input, as the cutoff frequency is varied. (L) Frequency-response gain plot for the same cutoff frequencies shown in (J). (M) Simulations predict a linear relationship between the low-pass filter's cutoff frequency and the mean delay time of Erk activation.

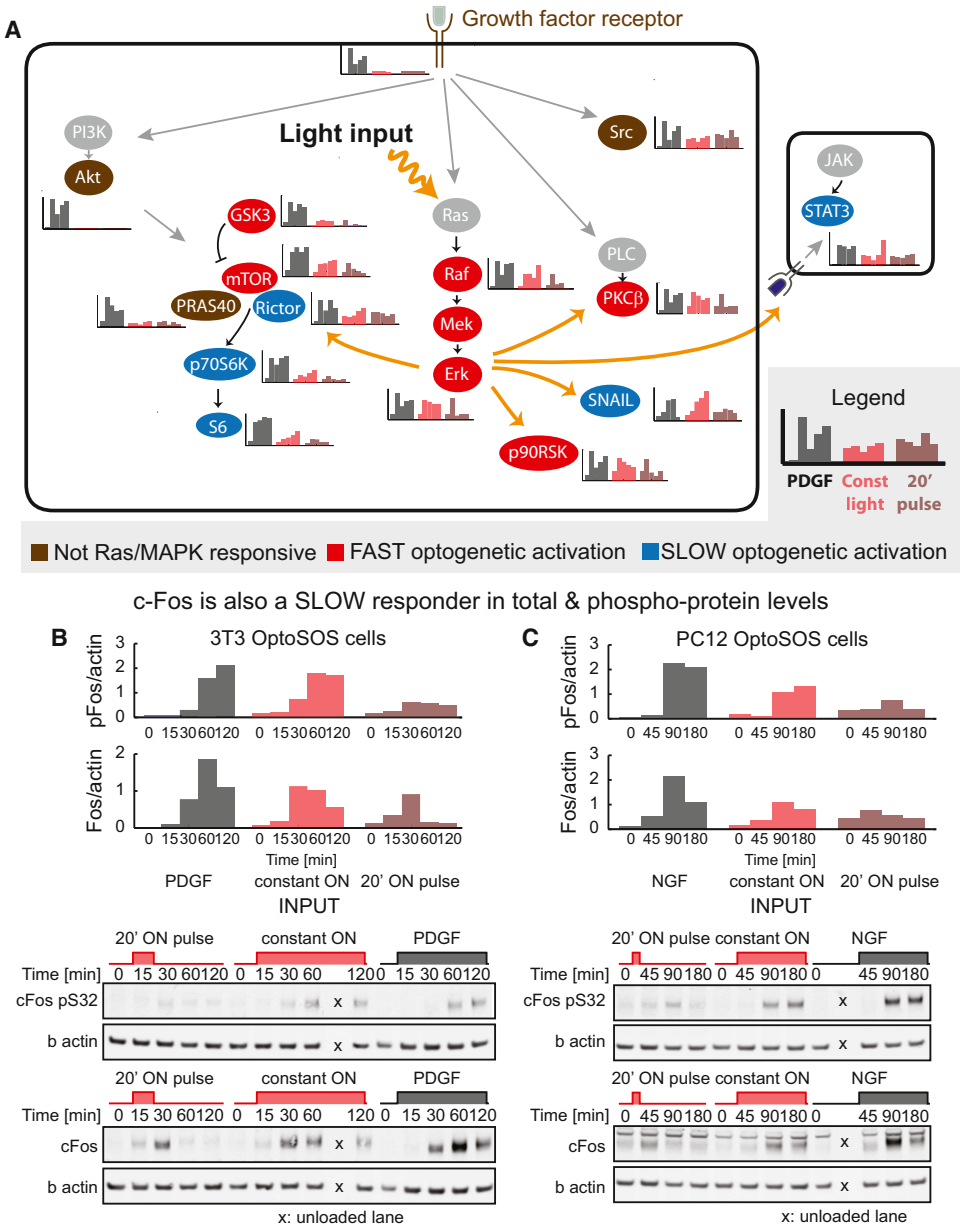

Figure S4. Time-Varying Optogenetic Ras Activity Is Decoded by Downstream Pathways, Related to Figure 5

(A) The dynamics of optogenetic Ras activation are decoded by a broad set of downstream pathways. Selected hits from the RPPA experiment are mapped onto a diagram of growth factor-mediated pathway activation. Nodes are highlighted that exhibit activation by PDGF but not light (brown circles), quickly track the dynamics of light-activated Ras (red), and respond selectively to sustained but not transient light inputs (blue). Nodes that were not measured by RPPA but are key pathway components are shown in gray. RPPA timecourse data is shown next to each corresponding node, as in Figure 5.

(B and C) Both total and phosphorylated c-Fos exhibit class III filtering, responding selectively to sustained light inputs. The NIH 3T3 lysates used in the RPPA experiment were Western blotted for phospho and total c-Fos (B). Additionally, lysates collected at various time points from PC12 opto-SOS cells after 100 ng/ml NGF stimulation, constant light, or a 20 min light pulse also show dynamic decoding by c-Fos (C).

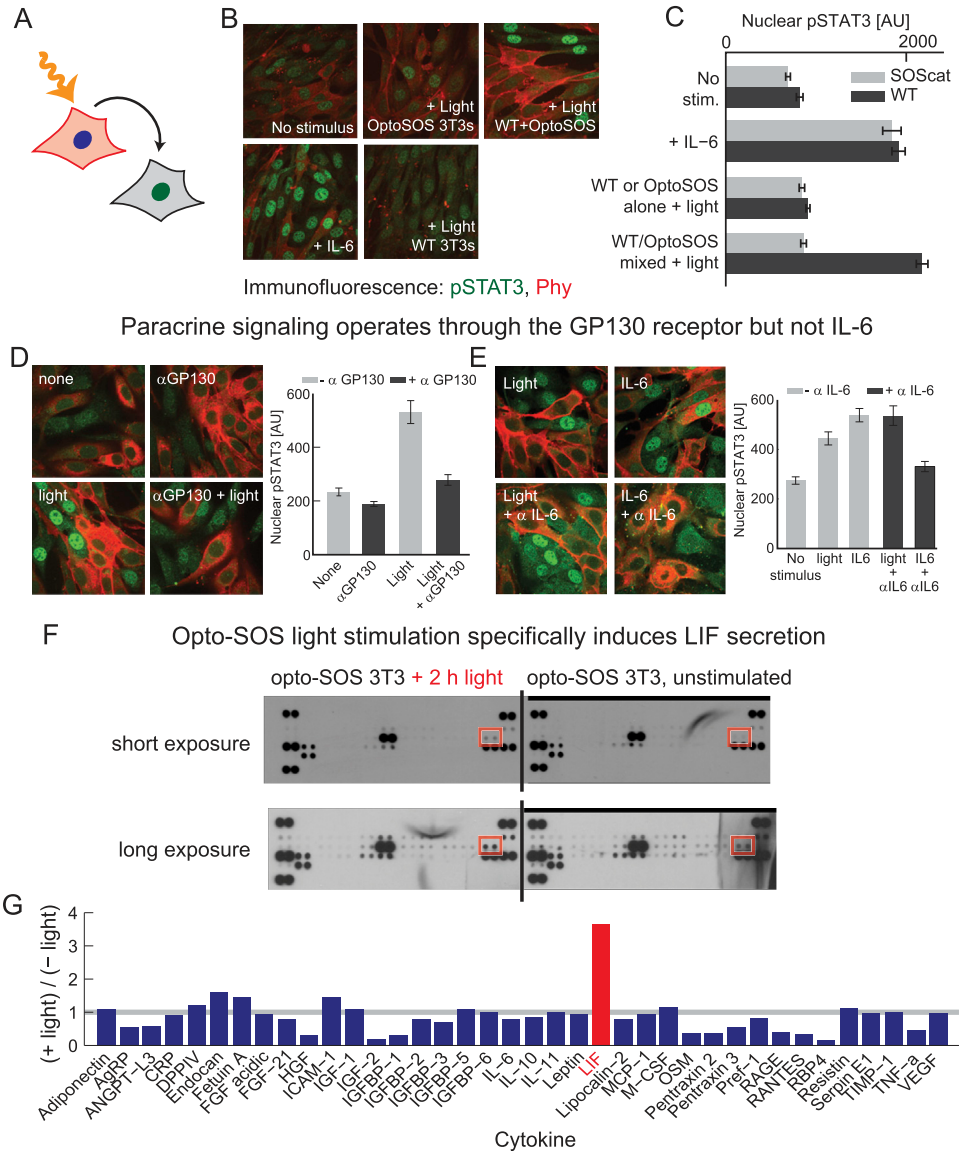

Figure S5. Dissecting the Paracrine Erk-to-STAT3 Signaling Arm, Related to Figure 6

(A) Light stimulation of Ras in 3T3 opto-SOS cells leads to STAT3 phosphorylation in cocultured WT 3T3 cells.

(B) Paracrine signaling was observed by immunofluorescence staining for phospho-STAT3 in WT/opto-SOS cocultures. Mixed populations of opto-SOS and WT 3T3s were left untreated (top left), treated with IL-6 (bottom left), or light (top right) for 2 hr. As controls, homogenous opto-SOS and WT cultures were stimulated with a 2 hr light input (middle panels). Membrane Phy-mCherry-CAAX expression (red) and nuclear phospho-STAT3 (green) are shown.

(C) Quantification of the nuclear phospho-STAT3 levels in at least 50 cells per condition shows that unstimulated or light-treated homogenous cultures do not accumulate nuclear phospho-STAT3, whereas WT 3T3s cocultured with light stimulated opto-SOS 3T3s activate high levels of phospho-STAT3, comparable to saturating IL-6 treatment. Mean + SEM are shown for each cell type and condition.

(D) Paracrine signaling operates through the GP130 cell surface receptor subunit, a class of cytokines known as the IL-6 family. Treatment with a GP130 neutralizing antibody blocks a paracrine response in a coculture of WT/opto-SOS 3T3s stimulated by 2 hr of light.

(E) IL-6 is not the IL-6 family cytokine responsible for paracrine signaling. A WT/opto-SOS 3T3 coculture treated with an IL-6 neutralizing antibody still showed a strong paracrine response despite the neutralizing antibody's ability to block exogenous IL-6. Quantification shows nuclear phospho-STAT3 in at least 50 WT cells per condition.

(F and G) A mouse cytokine array demonstrated that LIF is upregulated by light-stimulated opto-SOS 3T3s. Blot images (F) and quantification (G) are shown. After 2 hr of light stimulation, a 4-fold change in LIF was observed in the media.

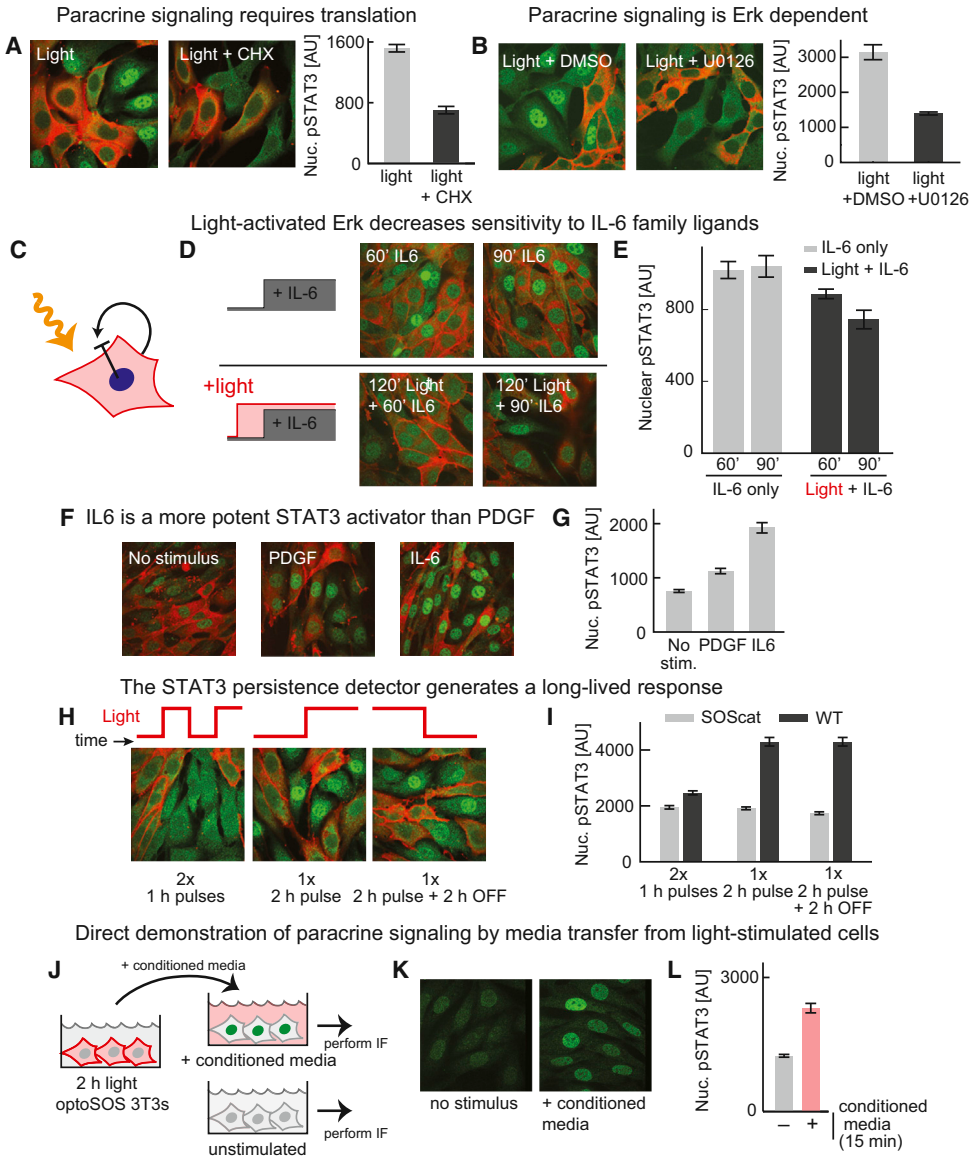

Figure S6. Elucidating the Dependencies of STAT3 Paracrine Activation and Intracellular Inhibition, Related to Figure 6

(A) Paracrine STAT3 signaling requires translation. Treatment by cycloheximide (CHX) strongly inhibits STAT3 activation in a WT/opto-SOS 3T3 coculture stimulated by 2 hr of activating light. Bar graphs show nuclear STAT3 in each condition across a population of at least 50 cells (mean + SEM).

(B) Paracrine STAT3 signaling is Erk-dependent. Treatment by the MEK inhibitor U0126 strongly inhibits STAT3 activation in a WT/opto-SOS 3T3 coculture stimulated by 2 hr of activating light. Bar graphs show nuclear STAT3 in each condition across a population of at least 50 cells (mean + SEM).

(C–E) Light inhibits sensitivity to IL-6 family cytokines in opto-SOS cells (illustrated in C). (D and E) Treatment of opto-SOS cells with IL-6 in the presence or absence of prestimulation by light demonstrates a decrease in opto-SOS cells' IL-6 sensitivity in a light-dependent manner. Representative immunofluorescence images (D) and quantification of at least 50 cells per condition (E) are shown (mean + SEM).

(F and G) Although PDGF also activates STAT3 phosphorylation (previously reported to act intracellularly through Src), this activation is much less potent than through IL-6 family cytokines. Immunofluorescence images (F) and quantification (G) of at least 50 opto-SOS cells per condition is shown (mean + SEM).

(H and I) STAT3 paracrine signaling depends on the persistence of Ras activation, not just the total amount of time where Ras is activated. Cells treated with two 1 hr pulses separated by a 1 hr delay activate less Ras than cells treated with a single 2 hr pulse. The paracrine signal is long-lived, as a 2 hr light stimulus followed by 2 hr of inactivating light does not diminish phospho-STAT3 levels. Representative immunofluorescence images (H) and quantification of at least 50 opto-SOS and WT 3T3s from each coculture (I) are shown (mean + SEM).

(J–L) Paracrine signaling can be demonstrated directly by transfer of conditioned media from light-stimulated cells to unstimulated naive cells. (J) Schematic of media transfer experiment. (K) Still images showing nuclear translocation of naive cells after transfer of media from light-stimulated cells. (L) Quantification of nuclear STAT3 from (K), mean of at least 50 cells (mean + SEM).